JOURNAL OF THERMOPHYSICS AND HEAT TRANSFER
Vol. 19, No. 2, April–June 2005

# Jet-Impingement Heat Transfer in Rotating Channels with Staggered Extraction Flow

James A. Parsons*
*Mississippi State University, Mississippi State, Mississippi 39762*
and
Je-Chin Han†
*Texas A&M University, College Station, Texas 77843-3123*

**The effect of orthogonal channel rotation on jet-impingement cooling by arrays of circular jets in two channels was studied. Impinging jet flows on smooth target walls were in the direction of rotation in one channel and opposite to the direction of rotation in the other channel. Spent air exited the channels through extraction holes, staggered with respect to the impinging jets, in each target wall, which eliminates crossflow on other jets. Experimental heat-transfer results for these target walls, for the jet walls containing the jet-producing orifices, and for the connecting sidewalls show that as the jet rotation number increases to 0.0028 these wall Nusselt numbers decrease to 35, 25, and 30%, respectively, below their corresponding nonrotating values. Jet rotation number is a correlating parameter, and as wall-to-jet temperature difference ratio increases to 0.129 the wall Nusselt numbers vary up to 10%. Comparisons are made with previous rotating results for target wall heating only and for the radially outward crossflow exit configuration.**

## Nomenclature

| | | |
|---|---|---|
| $A_{\text{wetted}}$ | = | exposed (wetted), heated plate surface area |
| $D$, $D_j$ | = | impingement jet orifice diameter −1.59 mm (0.0625 in.) |
| $D_e$ | = | extraction orifice diameter −2.54 mm (0.100 in.) |
| $F$ | = | fluid body forces as a result of rotation |
| $G$ | = | mass flux based on cross-sectional area of flow |
| $h$ | = | heat-transfer coefficient |
| $k$ | = | thermal conductivity of coolant (air) |
| $Nu$ | = | local Nusselt number ($hD/k$) for rotating conditions |
| $Nu_0$ | = | nonrotating local Nusselt number at corresponding location |
| $q_{\text{loss}}$ | = | heat-transfer rate from heated wall to test model |
| $q_{\text{total}}$ | = | total heat-transfer rate from heated wall |
| $Re_{\text{jet}}$ | = | average jet hole Reynolds number ($\rho_j \bar{V}_j D/\mu$) |
| $Ro$ | = | average jet rotation number ($\Omega D/\bar{V}_j$) |
| $r_m$ | = | radial distance from axis of rotation to test model's mean radius |
| $T_c$ | = | measured (and interpolated) coolant temperature in channels |
| $T_j$ | = | inlet or jet temperature, ≈21 to 27°C |
| $T_w$ | = | local wall (plate) temperature |
| $(T_w - T_j)/T_w$ | = | wall-to-coolant temperature difference ratio based on jet inlet temperature |
| $V$ | = | local velocity |
| $\bar{V}$ | = | average velocity |
| $X$ | = | radially outward distance from test model inlet |
| $\mu$ | = | air dynamic viscosity |
| $\rho$ | = | coolant density |
| $\Omega$ | = | rotational speed; rad/sec in Ro and forces, rpm in figures |

*Subscripts*

| | | |
|---|---|---|
| AFH | = | all film hole exit config. (100% extraction hole tests) |
| AW | = | sidewall A |
| BW | = | sidewall B |
| CEN | = | caused by centrifugal force |
| CH | = | channel |
| COR | = | caused by Coriolis force |
| JW | = | jet wall |
| $j$ | = | jet |
| TW | = | target wall |
| $w$ | = | wall (or plate) |
| XF | = | crossflow exit configuration |

Received 13 February 2004; revision received 13 August 2004; accepted for publication 13 August 2004. Copyright © 2003 by James A. Parsons and Je-Chin Han. Published by the American Institute of Aeronautics and Astronautics, Inc., with permission. Copies of this paper may be made for personal or internal use, on condition that the copier pay the $10.00 per-copy fee to the Copyright Clearance Center, Inc., 222 Rosewood Drive, Danvers, MA 01923; include the code 0887-8722/05 $10.00 in correspondence with the CCC.

*Assistant Professor, Department of Mechanical Engineering. Member AIAA.

†M.C. Easterling Chair Professor, Turbine Heat Transfer Laboratory, Department of Mechanical Engineering. Associate Fellow AIAA.

## Introduction

ADVANCED cooling designs for gas-turbine blades/buckets have considered impingement by arrays of jets among other methods such as film cooling and flow in internal channels with turbulated and/or roughened wall surfaces. The cooling of turbine components is necessary to meet component durability goals, but the extraction of coolant from the gas-turbine engine degrades performance. Thus a minimum amount of coolant must be used. The turbine designer needs to predict the coolant flow accurately, the internal and external blade/bucket heat transfer, and resulting local component temperatures and stresses. In lieu of reliable computational heat-transfer predictions for complicated flow situations like jet impingement, the designer relies on experimental results that closest match the cooling geometry and operating conditions. Blade/bucket rotation creates Coriolis, centrifugal, and buoyancy forces on these coolant flows that are not present for nonrotating conditions. These forces alter the coolant motion in direction and magnitude and thus the convective heat transfer on all of the walls that form the channel into which the jets flow. The goal of this investigation is to extend the understanding of internal jet-impingement cooling in channels for turbine blades/buckets under rotating conditions.

A complete list of known experimental studies in open literature follows for orthogonally rotating channels with jet-impingement cooling. Epstein et al.[1] showed results in the leading-edge region

for a single row of jets flowing perpendicular to direction of rotation with exit flow radially outward (creating crossflow on jets at larger radii). The heat transfer decreased up to 30% below the nonrotating results. Mattern and Hennecke,[2] using the naphthalene sublimation technique, also investigated the leading-edge region, but with flow exiting the channel in the blade/bucket chordwise direction. These results showed reductions up to 40%. Parsons and coworkers.[3–5] used the same test stand and same model as for the present study for jet impingement in channels at the midchord region with jet flow in and opposite to the direction of rotation. The exit flow configurations were crossflow radially outward (denoted XF) and through extraction holes (film cooling holes) in the target walls (AFH), whereas the wall thermal boundary conditions were target-wall-only heated (-TWH) and all four channel walls heated-target, jet, two sidewalls (-4WH): Parsons and Han[3] for XF-TWH, Parsons et al.[4] for XF-4WH, and Parsons and Han[5] for AFH-TWH. These papers also showed channel wall heat transfer deceases with rotation, the validity of jet rotation number as a correlating parameter, and the effect of varying the wall-to-jet temperature difference (jet buoyancy). This paper completes the preceding set for AFH-4WH. Akella and Han[6,7] also used the same test stand but a different test model with a two-pass radially outward and radially inward crossflow configuration and TWH. Because the jet-exit-to-target-wall and jet-to-jet spacings were reduced and the channel-flow-to-jet-flow mass flux ratio $G_c/G_j$ was greater compared to those for the present test model, as jet rotation number increased the decreases in target-wall heat transfer below the nonrotating results were not as large. Park et al.[8] did not study jet impingent but rather, using mass-transfer techniques, studied the effects of channel orientation, ribs, and flow ejection through holes in channel walls (effusion heat transfer) for rotating channels. Compared to rotating channels with through flow, trailing-wall enhancement and leading-wall degradation trends in wall heat transfer were reversed. There are numerous other stationary jet-impingement studies for jet spacing, target wall roughness, flow exit configuration, etc., and recently local results are obtained using liquid crystals and infrared thermometry. Because of turbulence and the three-dimensional nature of jet-impingement flow, computational methods have limited success in predicting jet-impingement heat transfer.

As compared to TWH, the 4WH thermal boundary condition is important for two reasons. The first is to determine how the target-wall heat-transfer coefficient changes between TWH and 4WH. Secondly, although jet impingement directly on the back side of a hot turbine component wall cools the wall, a significant amount of wall cooling is also provided by conduction through and the fin effect of the other walls surrounding the jet impingement channel: these other walls act as fins for the hot wall. It is the combined effects of all of the cooling techniques that determine the convective boundary conditions on the cooled and hot gas path sides, and of the component construction that determine the thermal-mechanical performance of hot turbine components. As just stated, rotation will alter flow and heat transfer on theses "fin" walls as compared to stationary results.

The film extraction exit configuration minimizes the degrading effects on heat transfer as a result of crossflow. Specifically, the goal is to measure pressures to determine flow distributions in and regional surface convective heat transfer on smooth target walls, jet walls, and side walls in rectangular cross-sectioned, orthogonally rotating, twin channels with impingement cooling by square arrays of circular jets. The spent air exits each twin channel through extraction orifices in the two target walls, and the jet hole and the extraction hole arrays are staggered. Nonrotating data will be taken to form a baseline and to compare with previous nonrotating investigations. Comparisons will be made with previous rotating impingement investigations.

## Experimental Apparatus and Test Procedure

This investigation uses the same test model, rig, and procedures as shown in figures and described in detail in Refs. 3–5. The new results presented here are for the flow exit and wall thermal boundary conditions, AFH-4WH, as just explained. Figure 1 shows the test model schematic for AFH, flows, and forces on the fluid flows. Because the tests for flow distribution are conducted adiabatically,

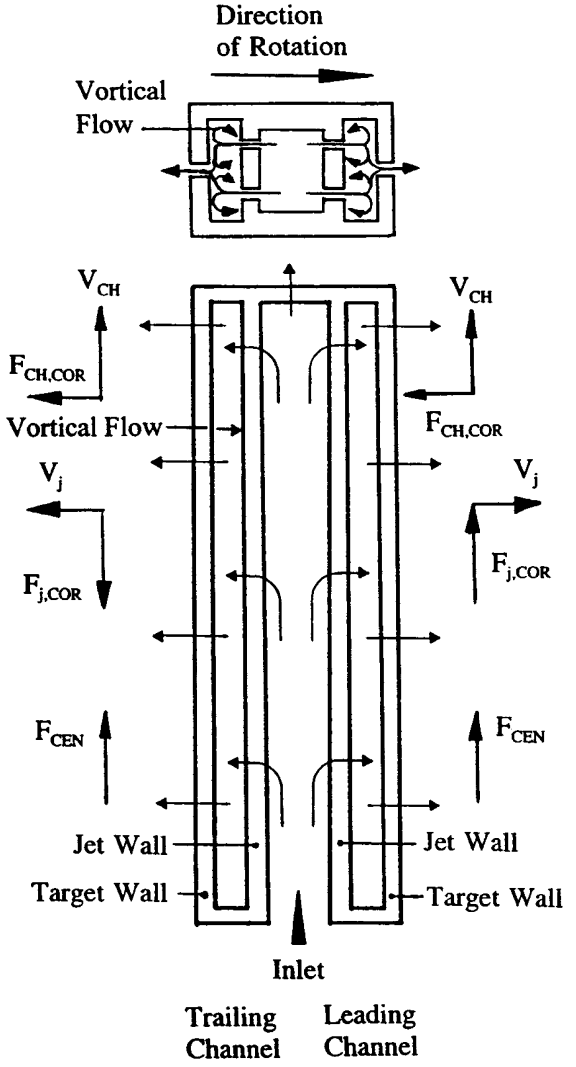


**Fig. 1 Test-model schematic for AFH including velocities and forces; view in plane of rotation and end view showing direction of rotation. Center of rotation is upstream of inlet.**

the results, discussions, and conclusions reached for the distributions of jet Reynolds number and channel flows are the same as those for Parsons and Han[5] and are not duplicated here.

For heat-transfer results, regional convective heat-transfer coefficient $h$ is defined as $h = (q_{\text{total}} - q_{\text{loss}})/[(A_{\text{wetted}}(T_w - T_c)]$, where $q_{\text{total}}$ is the heat generated in a copper plate for heat-transfer tests; $q_{\text{loss}}$ is the heat loss for a plate; $T_w$ is a plate temperature; and $T_c$ is a temperature for the coolant adjacent to the center of the heated plates, which is obtained by spacial interpolation between measured local air temperatures. Copper plates line all four sides (jet, target, and the two connecting side walls) of the leading and trailing channels for steady-state measurements. The heat-loss tests are also conducted in the same manner; however, the data reduction to account for heat loss is modified as compared to previous papers and is described next.

### Heat-Loss Effects from Heated Jet Walls

For the jet wall, the heat loss (heat to other than the jet wall wetted surfaces) increases during testing with coolant (air) flow in the supply channel as compared to heat loss for the heat-loss tests without airflow. This is because with the jet wall plates heated, heat energy transfers by conduction through the Teflon® (5.1 mm thick) that backs the jet wall and then by convection to the air in the supply channel. This has two main effects.

For the jet wall, the ratio of the conductive plate heat loss measured without supply channel flow to the total plate power at test

conditions increases slightly from 0.015 to 0.035 as jet Reynolds is reduced from $10^3$ to $5 \times 10^3$. But this conductive loss must be added to the supply channel convective heat loss. By using one-dimensional thermal resistance assumptions to calculate the heat loss through the backing Teflon to the developing through airflow in the center supply channel, the actual heat loss at stationary (nonrotating) test conditions can be up to 20% of the measured plate power at the beginning of the channels (next to the inlet at small $X/D$). As the supply channel location increases ($X/D$ increases), the supply channel through flow decreases as well as this convective heat loss. Besides convection to the through airflow in the supply channel, there is also convection to the flow entering each jet hole in the region immediately around each jet hole (effusion heat transfer). These two convective heat-transfer situations are the first effect that alters the jet wall heat-transfer results and will be discussed later. In addition, as the channel rotates the through-flow convective heat loss in the supply channel changes as a result of rotation-induced centrifugal and Coriolis forces. For the jet wall of the leading channel, this loss decreases slightly, whereas for the jet wall of the trailing channel this loss increases slightly. These changes in convective heat loss from the corresponding stationary values are slight ($\sim$10%) because the supply channel rotation numbers ($\Omega \times$ supply channel hydraulic diameter/$\bar{V}_{\text{SupplyChannel}}$) are less than 0.05 at the locations where the through-flow convective heat losses are significant.[9]

Next the supply channel air temperature rises because of this convective heat transfer. Thus the jet supply air is slightly heated after the $T_i$ measurement thermocouple. Also as the flow enters the jet holes, the jet air is again slightly heated as it passes through the part of the jet hole that is within the heated jet wall copper plate. (This jet hole heating is incorporated in the jet wall results.) In addition, after the jet air impinges on the target wall and circulates in the leading and trailing channels, the circulating air is heated more for four-wall heating than for target-wall only heating. Then this circulation air transfers heat to the incoming jet air through the circular shear layers surrounding the jets. Thus the actual temperature for the air entering the leading and trailing channels and impinging on the target walls is slightly higher for four-wall heating as compared to that for results from Parsons and Han[5] for target-wall only heating. Thus the second effect is to slightly reduce the target-wall heat transfer (and Nusselt number) for the four-wall heating case as compared to the target-wall-only heating case.

#### Heat-Transfer Effect from Four-Wall Heating

However this second effect is overridden because the local wall-to-coolant temperature difference is smaller (the local coolant temperature is higher) for the four-wall heating case as compared to that for the target-wall heating-only case. Because the definition of $h$ (and $Nu$) has this temperature difference in the denominator, target-wall heat-transfer results for the four-wall heating case are larger than those corresponding to the target-wall-only heating case. This increase in target-wall heat transfer for four-wall heating is true for both the film extraction and crossflow geometries.

The uncertainty of the local heat transfer depends on the net heat input ($q_{\text{total}} - q_{\text{loss}}$) to the coolant and the local wall-to-coolant temperature difference. This uncertainty increases with decreasing temperature difference and decreasing net heat input. Considering the method by Kline and McClintock,[10] the typical uncertainty in the Nusselt number is estimated less than 8% for $Re_{\text{jet}} = 10^3$. However, the maximum uncertainty could be up to 12% for $Re_{\text{jet}} = 5 \times 10^3$ at the largest radial location ($X/D = 138$). The heat conduction between a plate and its neighbors is estimated to be less than 1% of the net heat input for each of the plates at $Re_{\text{jet}} = 5 \times 10^3$. However, this percentage decreases to 0.5% at $Re_{\text{jet}} = 10^3$. For $Re_{\text{jet}} = 5 \times 10^3$, as the rotation rate increases from 0 to 800 rpm, the average ratio of the heat-loss power to the total-plate power increases from 0.09 to 0.16 for the target walls. At $Re_{\text{jet}} = 10^3$, the average ratio increases from 0.06 to 0.10 as rotation increases. The uncertainty in pressure differences decreases from 0.17% at $Re_{\text{jet}} = 5 \times 10^3$ to 0.11% at $Re_{\text{jet}} = 10^3$ of the maximum pressure difference for a jet Reynolds number. The uncertainties in calculation of the jet mass fluxes are about 2.5%.

## Results and Discussion

Nusselt-number distributions for jet impingement in rotating channels for this test model geometry depend on 1) the ratio of the test model's mean radius to jet diameter, 2) the ratio of local radial distance to jet diameter, 3) average jet Reynolds number, 4) Prandtl number, 5) jet rotation number, 6) wall-to-coolant temperature difference ratio, 7) jet flow direction with respect to rotation direction, 8) channel geometry (cross section and orientation), 9) exit flow configuration, and 10) wall thermal boundary condition. The functional relationship is expressed as $Nu = f(r_m/D, X/D, Re_{\text{jet}}, Pr, Ro, (T_w - T_j)/T_w$, jet direction, channel geometry, exit flow configuration, wall thermal boundary condition), where $Pr = 0.72$ and $r_m/D = 397$. Operating conditions are $Re_{\text{jet}} = 5 \times 10^3$ and $10^3$, and $\Omega = 0, 400$, and 800 rpm, combining to produce $Ro\ (= \Omega D/\bar{V}_j) = 0.0$, 0.0008, 0.0015, and 0.0028. For all four walls held at uniform temperature, the wall-to-coolant temperature difference ratio is 0.0855 for 0 rpm, 0.0855 for 400 rpm, and 0.0855 and 0.129 for 800 rpm. For the present results all extraction orifices are open (AFH-4WH) as compared to the results presented in Parsons and Han[5] for AFH-TWH and HFH-TWH (50% open extraction orifices). Air properties are at the average of the measured inlet and exit coolant temperatures.

#### Flow Distribution

Because all of the flow distribution tests are conducted adiabatically, the nonrotating and rotating flow results for AFH-4WH are the same as those for AFH-TWH and are reported in Parsons and Han.[5] For AFH the channel mass flux is uniform and nearly zero, whereas for XF the channel mass flux (crossflow) increases as the radial channel position $X/D$ increases. For both XF and AFH, the jet mass flux increases with $X/D$, but the amount of increase is larger for XF than for AFH and is larger as jet Reynolds number increases. The effect of rotation is relatively small and slightly increases the jet and extraction flows in the trailing channel while slightly reducing these flows in the leading channel, as compared to nonrotating results. The previously cited papers cover all of these details.

#### Heat Transfer

*Nonrotating Results*

Figures 2a–2d show nonrotating Nusselt numbers $Nu_{0,\text{AFH}}$ vs channel location ($X/D$) for all eight walls (four walls in the leading and four walls in the trailing channels), for the jet Reynolds numbers $5 \times 10^3$ and $10^3$, and at $(T_w - T_j)/T_w = 0.0855$. For each jet Reynolds number, the nonrotating Nusselt numbers are approximately constant with channel location and equal on average between corresponding leading and trailing channels. Also the Nusselt numbers for sidewall A are the same as for sidewall B (Figs. 2c and 2d) and those corresponding for sidewalls A and B for the XF exit configuration. Refer to Refs. 3–5 for heat-transfer comparisons. This confirms the nonrotating test model operates symmetrically for flow and heat transfer. And as $Re_{\text{jet}}$ increases, so do nonrotating Nusselt numbers. This is because as impingement jet flow and wall surface flow increase, the wall boundary layers thin, and heat transfer increases.

For the jet wall (Fig. 2b) as just explained in the data-reduction section, the Nusselt numbers are reduced from the initial calculations to account for the convective heat loss to the supply channel flow. There are no adjustments made for the effusion convection heat loss near each jet hole. For $X/D > 25$ these adjusted Nusselt numbers are about the same as $X/D$ increases. For $X/D < 25$, the leading and trailing jet wall Nusselt numbers are increased. It is guessed that this plate/heater acts as guard element with nonsymmetric boundary conditions. There is solid Teflon for $X/D < 0$, whereas there is an aluminum end cap for $X/D > 151$. The difference in material thermal conductivity (low vs high) can explain the increase at low $X/D$ and the lack of increase at high $X/D$. The increased Nusselt numbers for $X/D < 25$ cannot be explained by additional through-flow convection heat loss alone.

In comparing the Nusselt-number levels among the channels walls, the target walls are greatest, the adjusted jet walls are about

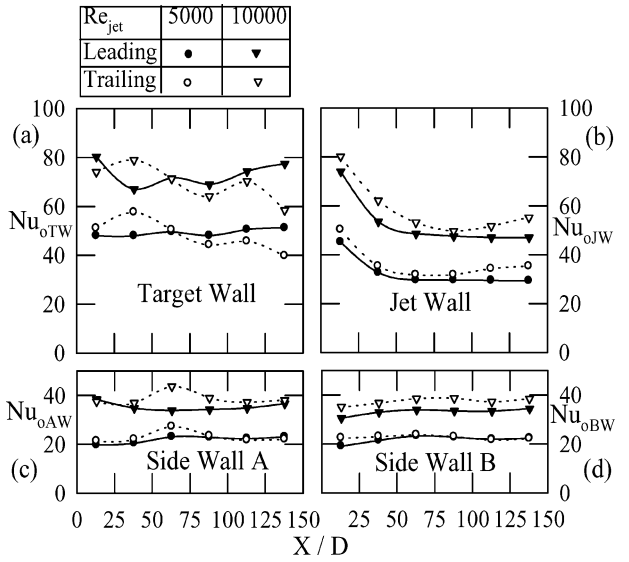


**Fig. 2 Nonrotating Nusselt number vs channel location for walls at $(T_w - T_j)/T_w = 0.0855$.**

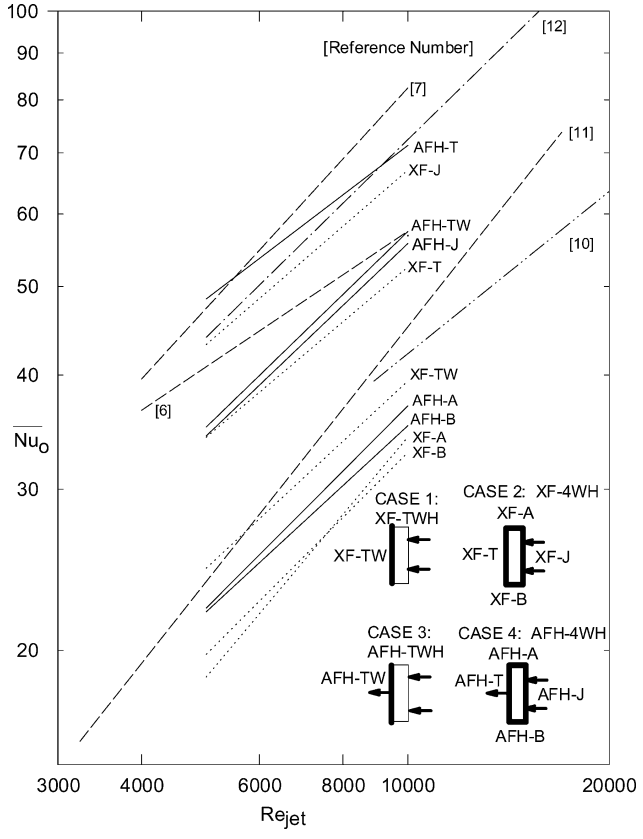


**Fig. 2e Average Nusselt number for nonrotation vs $Re_{jet}$ for present data and comparison with other investigations.**

70%, and the side walls are about 50%, respectively, of the corresponding target-wall results. These percentages are for a channel aspect ratio of 3 (channel transverse length 19.1 mm and jet travel distance 6.4 mm).

As $X/D$ increases for 4WH, the nonrotating target-wall Nusselt numbers for XF decrease from higher than the corresponding AFH results to lower than the corresponding AFH results at large $X/D$. However for TWH, the target-wall heat-transfer results have less variation with channel location. This is because crossflow bends jets away from the target wall and more so at large $X/D$, decreasing heat transfer as compared to the nearly uniform results for the AFH exit configuration.

To show the integrity of the experimental method and test model, bulk mean temperature rise calculated from an energy balance is within 10 and 30% of the measured local air temperature rise for $Re_{jet} = 5 \times 10^3$ and $10^3$, respectively.

Figure 2e shows the wall average of nonrotating Nusselt numbers $\bar{N}u_0$ vs $Re_{jet}$ and comparisons with other jet-impingement results. In Fig. 2e, case 1 is for XF-TWH Parsons and Han,[3] case 2 is for XF-4WH Parsons et al.,[4] case 3 is for AFH-TWH Parsons and Han,[5] and case 4 is for AFH-4WH, the present results. The legend shows the heated, active walls for each case. Figure 2e also shows target-wall results for Akella and Han[6] (smooth wall), for Akella and Han[7] (ribbed wall), and for other researchers.[11–13]

As just explained in the data-reduction section, the target-wall Nusselt numbers (Fig. 2e) for 4WH are larger than those corresponding for TWH. For the target wall, the TWH results are about 80% of those for 4WH and are ~70 and ~50 for $Re_{jet} = 10^3$ and $5 \times 10^3$, respectively.

For the side walls A and B of cases 2 and 4, the heat-transfer results are about equal for the A and B pairs of walls. The A and B wall results are lower than but also increase as $Re_{jet}$ increases at approximately the same rate as for the target and jet walls. As the exit flow configuration changes from AFH to XF, the side-wall Nusselt numbers decrease slightly. This is because for XF the fluid flow collects and is along the channel axis, which is away from the side walls. This slightly thickens the side-wall boundary layers for XF, as compared to AFH, and reduces XF side-wall heat transfer. Because the side walls are narrower (promoting thicker boundary layers) and do not have jets directed at them, the side-wall results are the lowest.

For XF, comparing cases 1 and 2 shows the effect of additional wall heating (TWH vs 4WH). For the target wall the 4WH heat-transfer results are increased as compared to the TWH results. This is because more heat energy overall transfers to the channel air for 4WH than for TWH. This increases the channel air temperature, decreases the wall to air temperature difference, and thus increases the target-wall heat transfer coefficient.

For AFH comparing cases 3 and 4 also shows the same effect of additional wall heating (TWH vs 4WH). As for XF, the target-wall AFH-4WH results are increased as compared to the AFH-TWH results for the same reasons already stated.

For TWH comparing cases 1 and 3 show the effect of exit flow configuration. The XF-TWH results are smaller than those for AFH-TWH. This is because the presence of crossflow bends the jets away from the target walls, reducing target-wall heat transfer.

For 4WH comparing cases 2 and 4 also show the same effect of exit flow configuration. The target wall XF-4WH results are also smaller than those for target-wall AFH-4WH and for the same reason as already stated. For the jet wall, the AFH results are adjusted (reduced) as just described in the data-reduction section while the XF results are not adjusted. The AFH-4WH jet wall results are less than those results corresponding to the AFH-4WH target wall. However for XF-4WH, the reverse is true; the XF-4WH jet wall results are more than those corresponding to XF-4WH target-wall results. Perhaps if the same jet wall adjustment were applied to the XF-4WH jet wall, the XF-4WH jet wall results would be more than but closer to or possibly less than those results for the XF-4WH target wall, the same as for the AFH-4WH results.

The jet geometry for Kercher and Tabakoff[11] also creates high crossflow, and thus their results are at the same level and follow the same trend as for XF-TWH. The results for Huang et al.[12] are also for a crossflow geometry and are similar. The jet geometry used by Florschuetz et al.[13] is widely spaced, and thus the Nusselt numbers are highest for smooth target walls because the crossflow effect is minimized. Akella and Han[7] results for ribbed target walls are highest of all.

*Rotating Results for AFH-4WH*

*Effect of rotation relative to nonrotation.* Figures 3a–3h show the effect of rotation on the local Nusselt-number ratio $Nu_{AFH}/Nu_{0,AFH}$. Note that the Nusselt-number ratio is the local Nusselt number divided by the corresponding measured local

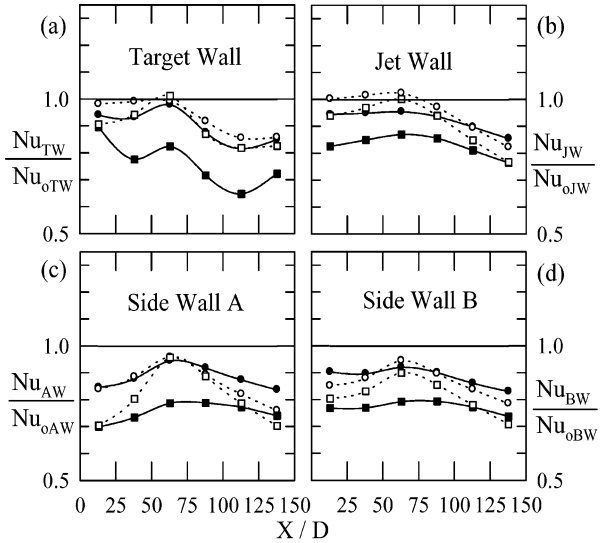


| $Re_{jet}$ | | 5000 | 5000 |
|---|---|---|---|
| rpm | 0 | 400 | 800 |
| Ro | 0 | 0.0015 | 0.0028 |
| Leading | — | • | ■ |
| Trailing | — | ○ | □ |

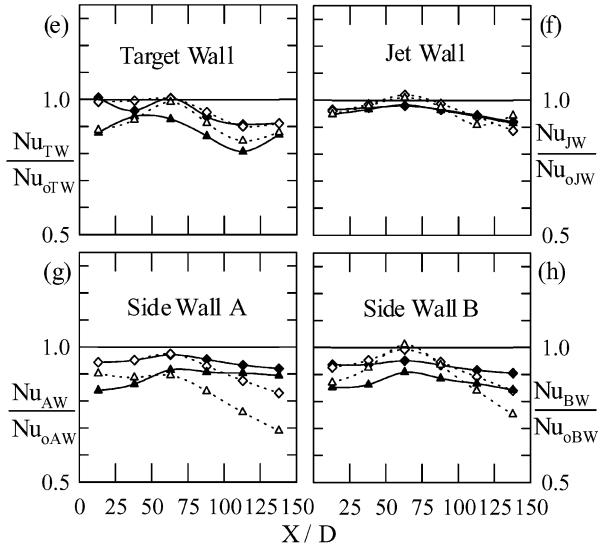


| $Re_{jet}$ | | 10000 | 10000 |
|---|---|---|---|
| rpm | 0 | 400 | 800 |
| Ro | 0 | 0.0008 | 0.0015 |
| Leading | — | ◆ | ▲ |
| Trailing | — | ◇ | △ |

**Fig. 3 Effect of rotation on wall Nusselt-number ratio at $(T_w - T_j)/T_w = 0.0855$: a–d) $Re_{jet} = 5 \times 10^3$; e–h) $Re_{jet} = 10^3$.**

Nusselt number for nonrotation (see Figs. 2a–2d). Figures 3a–3d show results at $Re_{jet} = 5 \times 10^3$ for a set of higher rotation numbers $Ro = 0.0$, 0.0015, and 0.0028 ($\Omega = 0$, 400, and 800 rpm, respectively) while Figs. 3e–3h show results at $Re_{jet} = 10^3$ for a set of lower rotation numbers $Ro = 0.0$, 0.0008, and 0.0015 ($\Omega = 0$, 400, and 800 rpm, respectively). Nondimensional parameter $Ro$ relates rotation effects and can be expressed as: the ratio of rotation speed $\times D/\bar{V}_j$ or (centrifugal force/jet Coriolis force) $\times$ ($D$/local radius from axis of rotation).

Figure 3a shows the target-wall Nusselt-number ratios decrease by up to 35% as compared to the nonrotating value of 1.0. For the leading channel, the jet, target-wall surface, and extraction hole velocities are reduced as compared to results for nonrotating target walls and for trailing channel walls under rotation. In addition, the centrifugal force combines with the jet Coriolis force to bend the jets away from the leading channel target wall. These thicken the boundary layers and decrease the heat-transfer coefficients. For the trailing channel, the jet, target-wall surface, and extraction hole velocities can increase as compared to nonrotating results, and the centrifugal force opposes the jet Coriolis force on the jets, which reduces jet bending. Thus, the decreases in Nusselt-number ratio are less for the trailing channel than those decreases for the leading channel. These decreases are greater for $X/D > 75$, where there are greater jet bending Coriolis and centrifugal forces than the decreases for $X/D < 75$. For 4WH, the target-wall Nusselt-number ratio decreases are slightly larger than those corresponding to the AFH-TWH.

Because there is little or no through crossflow (in the + or $-X$ direction) in the leading and trailing channels, there is also an absence of channel Coriolis forces directed at the target/jet walls that would have increased/decreased jet/target-wall heat transfer.

Figures 3b–3d show the jet wall, sidewall A and sidewall B Nusselt-number ratios decrease to 25, 30, and 30%, respectively, below the nonrotating value. As for the target wall, the Nusselt-number ratios for the jet wall and the side walls decrease as rotation rate increases from 0 to 400 and to 800 rpm. Also the decreases for the trailing channel Nusselt-number ratios are less than those for the leading channel as explained above.

Figures 3e–3h for $Re_{jet} = 10^3$ show Nusselt-number ratios for the target, jet, sidewall A, and sidewall B walls are between 1.0 and 0.80, 0.88, 0.70, and 0.75, respectively. Also at constant $Re_{jet} = 10^3$, as $Ro$ increases the differences between the Nusselt-number ratios for all walls and 1.0 increase. However, these differences for lower rotation numbers (Figs. 3e–3h) are reduced as compared to those differences at $Re_{jet} = 5 \times 10^3$ for higher rotation numbers (Figs. 3a–3d). As $Ro$ increases, the centrifugal force increases, thus bending jets away from the target walls, toward the center of the channels, and away from the other channel walls. This decreases heat transfer on all of the walls. Therefore the effect of rotation (to reduce Nusselt-number ratio) increases as $Ro$ increases. This is also true for AFH-TWH, XF-4WH, and XF-TWH.

*Effect of Reynolds number.* Figures 4a–4d show the effect of Reynolds number on Nusselt-number ratio while holding $Ro$ at 0.0015 for AFH-4WH. The rotation number is held constant by varying the rotation speed $\Omega$ and $\bar{V}_j$ (or $Re_{jet}$), that is, $\Omega = 400$ rpm, $Re_{jet} = 5 \times 10^3$, and $\Omega = 800$ rpm, $Re_{jet} = 10^3$. The results show the target, jet, and sidewall B Nusselt-number ratios are within 6% as either Reynolds number or rotation speed changes at constant rotation

| $Re_{jet}$ | 5000 | 10000 |
|---|---|---|
| rpm | 400 | 800 |
| Leading | • | ▲ |
| Trailing | ○ | △ |

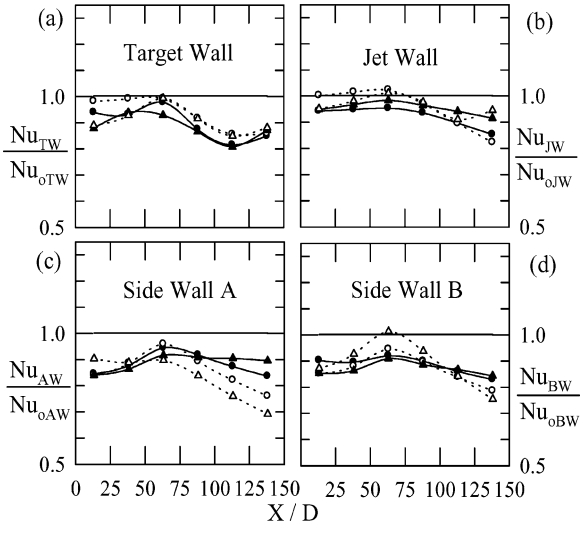


**Fig. 4 Effect of Reynolds number on wall Nusselt-number ratio.**

number for corresponding walls and channel locations. For sidewall A the difference in these ratios grows to 20% at large $X/D$. Thus it appears in general the rotation number remains a characteristic nondimensional parameter for rotating jet impingement. Closer differences (within 2%) are found for target-wall ratios for AFH-TWH and XF-TWH.

*Effect of wall-to-coolant temperature difference ratio.* Figures 5a–5d show the effect of the target wall-to-coolant temperature difference ratio $(T_w - T_j)/T_w$ on Nusselt-number ratio for $Re_{\text{jet}} = 5 \times 10^3$, $Ro = 0.0028$. Figures 6a–6d show the same effect but for $Re_{\text{jet}} = 10^3$, $Ro = 0.0015$. Figures 5a–5d and 6a–6d illustrate once again all of the Nusselt-number ratios vary within 35% below 1.0 as a result of the effect of rotation. Figures 5a–5d and 6a–6d also show as the wall-to-coolant temperature difference ratio increases from 0.0855 to 0.129 the maximum differences between

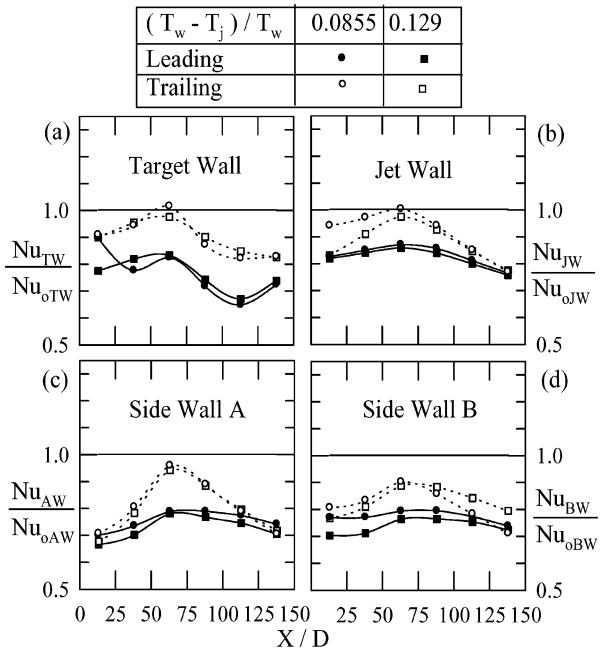


**Fig. 5 Effect of wall-to-coolant temperature difference ratio on wall Nusselt-number ratio; $Re_{\text{jet}} = 5 \times 10^3$.**

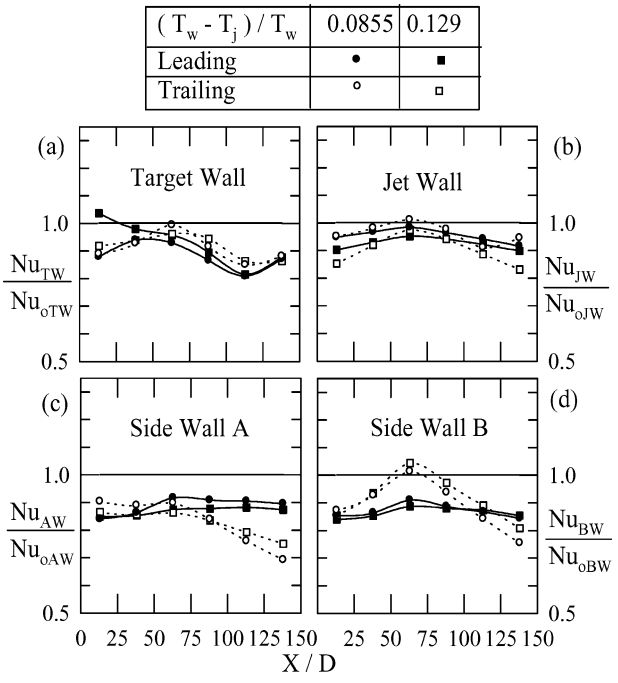


**Fig. 6 Effect of wall-to-coolant temperature difference ratio on wall Nusselt-number ratio; $Re_{\text{jet}} = 10^3$.**

corresponding Nusselt-number ratios are less than 6% regardless of wall, channel, channel location, and rotation number. For XF-4WH, the maximum difference is 10%, whereas for AFH-TWH and XF-TWH the maximum target-wall difference is less than 5%. The jet, vortical, and secondary flows and their corresponding Coriolis forces are in many directions and thoroughly mix the air in the channels. This produces small local variations of temperature and density. Recall the buoyancy body force $[\Delta\rho_{\text{local}}\,(\Omega^2 r + \Omega V_{\text{local}})]$ depends on local density variation. Thus as wall-to-coolant temperature difference ratio and thus local temperature and density variation increase, the effects of buoyancy forces remain small and are in the same directions as those for local centrifugal and Coriolis forces.

Figure 5 at $Re_{\text{jet}} = 5 \times 10^3$ shows that the Nusselt-number ratios for the leading channel are less than those corresponding for the trailing channel. This is also true for $Re_{\text{jet}} = 5 \times 10^3$ and AFH-TWH. However for $Re_{\text{jet}} = 5 \times 10^3$ and both XF-4WH and XF-TWH, the Nusselt-number ratios for the trailing channel are less than those corresponding for the leading channel. It is believed for $Re_{\text{jet}} = 5 \times 10^3$ that the lower leading channel results for AFH are caused by reduced jet flows in the leading channel under rotation while the lower trailing channel results for XF are caused by reduced jet flows in the trailing channel under rotation, both as compared to corresponding nonrotating jet flows. It is thought that the rotation of the test model alters the jet flow. However at $Re_{\text{jet}} = 10^3$ the rotation effect on jet flow is reduced. Close examination of results for AFH-4WH, AFH-TWH, XF-4WH, and XF-TWH show that although jet flows are comparable and as $(T_w - T_j)/T_w$ increases, XF heat-transfer ratios decrease very slightly while AFH heat-transfer ratios vary, with other parameters constant. This might be explained as follows. For XF the relative buoyancy force for warm fluid next to the heated walls is radially inward opposing the XF fluid flow and centrifugal force. This slightly thickens the wall boundary layers as compared to those for AFH, decreasing heat transfer.

*Effects of rotation number at selected channel locations.* Previous TWH papers show the target-wall Nusselt-number ratio vs rotation number at several $X/D$ channel locations. As just explained, as rotation number increases the Nusselt-number ratios decrease. These figures are similar for the 4WH results but are not presented. The maximum ratio decrease is up to 40% below the nonrotating result and occurs on sidewall A for 4WH for both AFH and XF. Finally as rotation number increases, the differences between ratios for the leading channel walls and the ratios for trailing channel walls increase for 4WH also, and these differences increase more for AFH than for those for XF.

Limited comparisons of the results of this test model to those results in Akella and Han[6,7] are made in those references. The jet rotation number range for the present data is much smaller than in those references. However the trend of decreasing Nusselt-number ratios as jet rotation number increases is the same as for XF-TWH Parsons and Han.[3] But the decrease is not as large for Akella and Han. For Akella and Han the jets are bigger (jet-area-to-plate-area ratio) and shorter (jet-to-target wall distance/jet diameter) than those of the present study. Thus they are more resistant to bending. Also the channel-to-jet-flow ratio $G_c/G_j$ is larger for Akella and Han, which dominates the bending of the jets. Thus the jet bending effects caused by rotation are relatively less for Akella and Han as compared to those for the present study.

The jet Coriolis and the centrifugal forces bend the jets away from the target walls and reduce wall heat transfer as compared to corresponding nonrotating results in the leading-edge[1,2] and midchord regions, and for crossflow (radially outward and inward[6,7]), transverse,[2] and film extraction exit flow configurations. For turbine blade/buckets, many forces (with parameters affecting magnitude/direction) affect jet impingement coolant motion and thus heat transfer. These body and surface forces include inertia (depending on density, local fluid speed; in the local flow direction); centrifugal (depending on density, rotation radius, rotation speed$^2$; in the radial direction); Coriolis (depending on density, rotation speed, local fluid speed; direction depends on local velocity and direction of rotation); buoyancy (depending on local density differences, centrifugal and Coriolis force magnitudes; in the centrifugal-radial and Coriolis

force directions); pressure (many magnitudes; many directions); and viscous (local fluid gradients; opposing local flow direction). The Reynolds number relates jet inertia to viscous forces, the rotation number relates centrifugal to jet Coriolis forces (not local Coriolis force) or rotation speed to jet speed, the rotational Grashoff number relates centrifugal buoyancy to viscous forces, and the wall-to-jet-temperature-difference ratio relates wall-to-jet densities (not local density differences). The actual force magnitudes and directions at engine operating conditions are much larger and possibly at slightly different relative directions than those tested in this study; not all relative ratios of forces (and directions) were duplicated simultaneously. The Coriolis forces are particularly difficult to model. Care must be used in applying these results to actual blade/bucket operating conditions because huge rotation forces can combine with small changes in a nondimensional parameters to create significant effects. However it is believed that the main effects of rotation on jet-impingement heat transfer have been measured by these investigations and confirmed by other researchers.

## Conclusions

For a square array of jets impinging normally on one target wall in a rectangular channel with staggered extraction through the target walls as the exit condition, jet flow velocities increase slightly as $X/D$, the radial channel location, increases. For a given jet Reynolds number, the pressure and thus flow distributions for rotation differ slightly from those without rotation. Under rotation jet flows toward the leading channel target wall are slightly reduced as compared to jet flows toward the trailing channel target wall. At constant jet Reynolds number and nonrotating conditions, as $X/D$ increases, the leading- and trailing-wall Nusselt numbers are nearly equal and constant. Nusselt numbers increase with jet Reynolds number. As rotation number ($\Omega D/\bar{V}_j$) increases up to 0.0028, the target, jet, and side-wall Nusselt-number ratios (Nusselt number for rotation/Nusselt number for corresponding nonrotating conditions) for the leading (jet flow in the direction of rotation) and trailing (jet flow opposite to the direction of rotation) channels decrease to 35, 25, and 30%, respectively, below the nonrotating value of 1.0. As wall-to-coolant temperature difference ratio $(T_w - T_j)/T_w$ increases from 0.0855 to 0.129 under rotating conditions, the wall Nusselt-number ratios vary up to 6%. For parameter ranges in this paper, varying the jet Reynolds number and rotation rate with $Ro$ constant had a small effect on wall Nusselt-number ratios for both channels; $Ro$ is a correlating parameter.

## Acknowledgments

This paper was supported in part by General Electric Aircraft Engines with C. Pang Lee as the project monitor.

## References

[1]Epstein, A. H., Kerrebrock, J. L., Koo, J. J., and Preiser, U. Z., "Rotational Effects on Impingement Cooling," *Proceedings of the First International Symposium on Transport Phenomena*, Heat Transfer and Fluid Flow in Rotating Machinery, Hemisphere Publ. Corp., Honolulu, HI, 1987, pp. 86–102.

[2]Mattern, C., and Hennecke, D. K., "Influence of Rotation on Impingement Cooling," *Proceedings of the 1996 International Gas Turbine and Aeroengine Congress and Exhibition—TurboExpo '96*, American Society of Mechanical Engineers (International Gas Turbine Inst.) New York, 1996.

[3]Parsons, J. A., and Han, J. C., "Rotation Effect on Jet Impingement Heat Transfer in Smooth Rectangular Channels with Heated Target Walls and Radially Outward Cross Flow," *International Journal of Heat and Mass Transfer*, Vol. 41, No. 13, 1998, pp. 2059–2071.

[4]Parsons, J. A., Han, J. C., and Lee, C. P., "Rotation Effect on Jet Impingement Heat Transfer in Smooth Rectangular Channels with Four Heated Walls and Radially Outward Cross Flow," *Journal of Turbomachinery*, Vol. 20, 1998, pp. 79–85; also *Proceedings of the 1996 International Gas Turbine and Aeroengine Congress and Exhibition—TurboExpo '96*, American Society of Mechanical Engineers (International Gas Turbine Inst.) Atlanta, 1996.

[5]Parsons, J. A., and Han, J. C., "Rotation Effect on Jet Impingement Heat Transfer in Smooth Rectangular Channels with Film Coolant Extraction," *International Journal of Rotating Machinery*, Vol. 7, No. 2, 2001, pp. 87–103.

[6]Akella, K. V., and Han, J. C., "Impingement Cooling in Rotating Two-Pass Rectangular Channels," *Journal of Thermophysics and Heat Transfer*, Vol. 12, No. 4, 1998, pp. 582–588.

[7]Akella, K. V., and Han, J. C., "Impingement Cooling in Rotating Two-Pass Rectangular Channels with Ribbed Walls," *Journal of Thermophysics and Heat Transfer*, Vol. 13, No. 3, 1999, pp. 364–371.

[8]Park, C. W., Yoon, C., and Lau, S. C., "Local Heat (Mass) Transfer in a Rotating Square Channel with Ejection Holes," *Journal of Thermophysics and Heat Transfer*, Vol. 12, No. 4, 1998, pp. 589–595.

[9]Wagner, J. H., Johnson, B. V., and Kopper, F. C., "Heat Transfer in Rotating Serpentine Passages with Smooth Walls," *Journal of Turbomachinery*, Vol. 113, No. 3, 1991, pp. 321–330.

[10]Kline, S. J., and McClintock, F. A., "Describing Uncertainties in Single-Sample Experiments," Mechanical Engineering, Jan. 1953, pp. 3–8.

[11]Kercher, D. M., and Tabakoff, W., "Heat Transfer by a Square Array of Round Air Jets Impinging Perpendicular to a Flat Surface Including the Effect of Spent Air," *Journal of Engineering for Power*, Vol. 92, Jan. 1970, pp. 73–82.

[12]Huang, Y., Ekkad, S., and Han, J. C., "Detailed Heat Transfer Distribution Under an Array of Orthogonally Impinging Jets," *Journal of Thermophysics and Heat Transfer*, Vol. 12, No. 1, 1998, pp. 73–79.

[13]Florschuetz, L. W., Truman, C. R., and Metzger, D. E., "Streamwise Flow and Heat Transfer Distributions for Jet Array Impingement with Cross Flow," *Journal of Heat Transfer*, Vol. 103, No. 2, 1981, pp. 337–342.